pp. 1–14 (2021)

Numerical evaluation of the effectiveness of coronary revascularization

S. S. Simakov[*†‡], T. M. Gamilov[*†§], F. Liang[§¶], D. G. Gognieva[‡], M. K. Gappoeva[‡], and P. Yu. Kopylov[§]

Abstract — In the present paper we construct the model of coronary flow which utilizes the patient's CT data on both large CA and perfusion. We reconstruct large coronary vessels based on the CT data and extrude possibly invisible vessels from the branches of the left coronary artery so that every terminal point supply every of standardized zone of myocardium. We apply a previously developed and validated 1D model of haemodynamics. Utilizing the patient-specific CTP data for modifying outflow terminal resistance at rest and under stress conditions is the major novelty of the present work. From our results it follows that acceptable values of fractional flow reserve (FFR) after the stenotic treatment may produce false negative output. Therefore healthy FFR values may be observed after ineffective revascularization. We also conclude that microvascular perfusion impairment plays significant role in correct computational estimation of haemodynamic indices before stenotic treatment. The advantage of the presented approach is the availability of transmural perfusion ratio assessment in everyday practice.

Keywords: 1D haemodynamics, coronary circulation, stenosis, myocardial perfusion, boundary conditions, fractional flow reserve, coronary flow reserve, instantaneous wave-free ratio, transmural perfusion ratio.

MSC 2010: 65D25, 37M05, 92B99

Coronary artery disease (CAD) remains the leading cause of disability or death in adults worldwide. Computed tomography angiography (CTA) has become an established diagnostic technique to assess the severity of CAD. Catheter-based fractional flow reserve (FFR) is currently regarded as the reference for the assessment of the haemodynamic severity of CAD [18] and indication for stent placement. The FFR value equals the pressure ratio after (distal to) stenosis to the pressure before the

[*]Marchuk Institute of Numerical Mathematics of the Russian Academy of Sciences, Moscow 119991, Russia

[†]Moscow Institute of Physics and Technology, Dolgoprudny 141701, Russia

[‡]Sechenov University, Moscow 119991, Russia. E-mail: simakov.ss@phystech.edu

[§]World–Class Research Center 'Digital biodesign and personalized healthcare', I. M. Sechenov First Moscow State Medical University (Sechenov University), Moscow 119991, Russia

[¶]Department of Engineering Mechanics, School of Naval Architecture, Ocean and Civil Engineering, Shanghai Jiao Tong University, 200240 Shanghai, China

The research was supported by the joint RSF-NSFC project (Russian Science Foundation, grant No. 21-41-00029 and National Natural Science Foundation of China, grant No. 12061131015).

stenosis (or aortic pressure) under the drug-enabled maximum hyperemia of the coronary vessels. FFR characterizes the maximum possible pressure recovery in the large coronary arteries (CAs) after stenting. Stenosis with FFR below 0.8 is haemodynamically significant and requires stenting or similar invasive treatment. Other valuable indices are coronary flow reserve (CFR) and instantaneous wave-free ratio (iFR). The CFR value equals the ratio of coronary blood flow (CBF) during drug-enabled maximum hyperemia to the CBF at rest [14]. CFR characterizes the maximum possible blood flow recovery in the large CAs after stenting. Unfortunately, CFR measurements are rarely possible in everyday clinical practice. iFR is measured in normal nonhyperemic conditions. iFR isolates a specific period in diastole, called the wave-free period, and uses the ratio of distal coronary pressure to the pressure observed in the aorta over this period [22]. This index does not involve administering a vasodilating drug but depends on the accurate estimation of the wave-free period. All haemodynamic indices — FFR, CFR, and iFR — characterize the severity of a lesion in a large (more than 0.5 mm in diameter) CA.

In general, there are two major sources of CAD. The first is stenosis of CAs. The second is impaired microcirculation of the myocardium. Stenosis in CA typically decreases blood supply to the heart tissue, damaging microcirculation of the myocardium. Thus, a correlation between CA stenosis and microcirculation failure certainly exists [1, 27]. However, this correlation is inexplicit [20]: a low FFR value may be a reason for the recommendation of CA stenting which will recover blood flow in large coronary arteries located downstream of the stenosis, but the myocardium perfusion still may be low due to the impaired microcirculatory region downstream. Thus, the revascularization will not be effective in this case. A lot of clinical studies investigate perfusion indices [6, 13, 19] or combine FFR with perfusion assessments [5, 15]. Modern mathematical models of coronary circulation rarely incorporate perfusion data for CAD evaluation [12, 17]. A lot of works consider FFR, CFR, or iFR regardless of the state of the microvessels in the myocardium [2, 3, 8].

Myocardial CT perfusion (CTP) allows for an evaluation of the impairment of myocardial microcirculation and ischemia [21]. CTP analysis is performed after administration of iodinated contrast through a catheter by imaging the left ventricular (LV) myocardium during the first pass of the contrast bolus. Iodinated contrast attenuates X-rays proportionally to the iodine content in tissue. Thus, myocardial perfusion defects can be directly visualized as hypoattenuating or non-enhancing regions. The increased blood flow conditions (hyperemia) allows revealing more perfusion abnormalities. Thus, a CTP dataset typically contains rest and stress (hyperemic) conditions.

In the present work, we construct the model of coronary flow, which utilizes the patient's CT data on both large CA and perfusion. We reconstruct large coronary vessels based on the CT data and extrude possibly invisible vessels from the branches of the left coronary artery so that every terminal point supplies every of the sixteen standardized zones of myocardium. We apply previously developed and validated 1D model of haemodynamics, which accounts for variable heart rhythm [9],

and distribute terminal hydraulic resistance based on the diameters of the parent vessels and Murray's law by a recursive algorithm. In our model, the terminal resistance is decreased according to a transmural perfusion ratio (TPR) increase. First, we demonstrate that TPR data improves the accuracy of FFR assessment. Second, we analyze the sensitivities of FFR, CFR, and iFR in the stenosed region to the degree of microcirculation damage by decreasing TPR and, thus, increasing local terminal resistance downstream and in collateral terminals. Utilizing the patient-specific CTP data for modifying outflow terminal resistance is the major novelty of the present work. We observe that in the presence of a stenosis, the downstream TPR value substantially change all haemodynamic indices (FFR, CFR, and iFR). The change of TPR in collateral terminals produces no substantial effect on FFR, CFR, and iFR. One may observe the same behaviour in a healthy network (without stenosis) and decreased TPR downstream.

From our results it follows that acceptable values of FFR after the stenotic treatment may produce false negative output. Therefore healthy FFR values may be observed after ineffective revascularization. Finally, we conclude, that microvascular perfusion impairment plays significant role in correct computational estimation and interpretation of haemodynamic indices across the stenotic regions of CAs before stenotic treatment.

1. Methods

1.1. Coronary circulation model

The vascular network consists of a synthetic aortic root, aorta and two patient-specific coronary arteries (left coronary artery (LCA) and right coronary artery (RCA)) with their branches. The aortic root and the aorta produce physiological boundary conditions. All arterial segments were modelled as thin, elastic tubes of a constant length. The cross-sectional area of each tube depends on blood pressure. The blood flow in the coronary vascular network and the aorta is simulated by a 1D model of the unsteady axisymmetric flow of Newtonian viscous incompressible fluid through the network of elastic tubes. The 1D haemodynamic model is derived from Navier–Stokes equations [23, 26]. The time-dependent heart outflow function and terminal resistance of the coronary network adopt the general haemodynamic model to the coronary circulation [9, 10, 11]. The model is described briefly as follows. The flow in every vessel satisfies the mass and momentum balances

$$\frac{\partial \mathbf{V}}{\partial t} + \frac{\partial \mathbf{F}(\mathbf{V})}{\partial x} = \mathbf{G}(\mathbf{V}) \tag{1.1}$$

$$\mathbf{V} = \begin{pmatrix} A \\ u \end{pmatrix}, \quad \mathbf{F}(\mathbf{V}) = \begin{pmatrix} Au \\ \dfrac{u^2}{2} + \dfrac{p(A)}{\rho} \end{pmatrix}, \quad \mathbf{G}(\mathbf{V}) = \begin{pmatrix} 0 \\ -8\pi\mu \dfrac{u}{A} \end{pmatrix}$$

where t is the time, x is the distance along the vessel counted from the vessel junction point, $\rho = 1.060\,\mathrm{kg/m^3}$ is the blood density, $A(t,x)$ is the vessel cross-section area,

p is the blood pressure, $u(t,x)$ is the linear velocity averaged over the cross-section, $\mu = 2.5$ mPa·s is the dynamic viscosity of the blood. The relationship between pressure and cross-section is defined by wall-state equation

$$p(A) = \rho_w c^2 \left(\exp\left(\frac{A}{\widetilde{A}} - 1 \right) - 1 \right) \tag{1.2}$$

where ρ_w is the vessel wall density (constant), c is the velocity of small disturbances propagation in the material of the vessel wall, $\widetilde{A}$ is the cross-sectional area of the unstressed vessel. At the vessel junction points we impose the mass conservation condition and the total pressure continuity

$$\sum_{k=k_1,k_2,\ldots,k_M} \varepsilon_k A_k\left(t,\widetilde{x}_k\right) u_k\left(t,\widetilde{x}_k\right) = 0 \tag{1.3}$$

$$p_k\left(A_k\left(t,\widetilde{x}_k\right)\right) + \frac{\rho u^2\left(t,\widetilde{x}_k\right)}{2} = p_{k+1}\left(A_{k+1}\left(t,\widetilde{x}_{k+1}\right)\right) + \frac{\rho u^2\left(t,\widetilde{x}_{k+1}\right)}{2} \tag{1.4}$$
$$k = k_1, k_2, \ldots, k_{M-1}$$

where k is the index of the vessel, M is the number of the connected vessels, $\{k_1,\ldots,k_M\}$ is the range of the indices of the connected vessels, $\varepsilon = 1, \widetilde{x}_k = L_k$ for incoming vessels, $\varepsilon = -1, \widetilde{x}_k = 0$ for outgoing vessels.

The boundary conditions at the aortic root include the blood flow from the heart, which is set as a predefined time function $Q_H(t)$:

$$u(t,0)A(t,0) = Q_H(t) \tag{1.5}$$

$$Q_H(t) = \begin{cases} \mathrm{SV}\dfrac{\pi}{2\tau}\sin\left(\dfrac{\pi t}{\tau}\right), & 0 \leqslant t \leqslant \tau \\ 0, & \tau < t \leqslant T \end{cases} \tag{1.6}$$

where SV is the stroke volume of the left ventricle, T is the period of the cardiac cycle, τ is the duration of the systole. Inflow parameters SV, T, and τ are extracted from patient's data. Section 1.2 presents details on defining terminal resistance at the outflow of peripheral arterial segments.

Stenosis is simulated as a separate vessel with a decreased diameter corresponding to patient's data. A decreased terminal resistance simulates hyperemia. FFR is calculated as a ratio between average pressure downstream stenosis and average aortic pressure during hyperemia. CFR is calculated as a ratio between hyperemic blood flow through stenosis to the blood flow through the same stenosis in patient quiet conditions (also referred to as the rest conditions). iFR is calculated as the ratio between average pressure after stenosis and average aortic blood pressure during the diastolic wave-free period (WFP) under the nonhyperemic normal condition. WFP begins in 25% of the way into diastole and ends 5 ms before the end of diastole following the general definition of iFR [22].

1.2. Outflow boundary conditions

We use the patient-specific CTP data which characterize the myocardium perfusion to define peripheral resistance more accurate. CTP images present the brightness of the iodinated contrast agent, which was administrated to the arterial blood and transferred through the microcirculation. The brightness of the contrast has no direct physiological meaning, but it is proportional to the volumetric blood flow and the oxygen delivery to tissue. Brighter regions correspond to a higher concentration of the contrast, and faint regions correspond to a lower concentration of the contrast. CTP workstation automatically divides a myocardium from inner to external surface into three layers: subendocardium, midwall, and subepicardium. It also divides the surface of every layer into the sixteen standardized zones (territories) as shown in Fig. 1. The embedded data processing software calculates the mean attenuation density (AD) of each myocardial layer in every zone. AD characterizes the impairment of the perfusion in a particular territory by the transmural perfusion ratio (TPR)

$$\mathrm{TPR} = \frac{AD_{\mathrm{end}}}{AD_{\mathrm{ep}}} \tag{1.7}$$

where AD_{end} is subendocardial AD and AD_{ep} is subepicardial AD. Two available datasets presented TPR measurements at the rest and stress states. The rest state corresponds to quiet patient conditions. The stress state is a state with increased blood flow. The stress state is activated by administration of the vasodilating agent (adenosine) which increases the lumen of the vessels and, thus, decreases the hydraulic resistance. The measured rest and stress TPR values for each territory are presented in Table 1. The FFR simulations require stress values; the iFR simulations rest values; the CFR simulations require both rest and stress values.

TPR has no direct physiological interpretation. However, it improves the overall diagnostic performance of CT-MPI in clinics [4]. TPR typically ranges from 0.0 to 1.4. Acceptable healthy values are between 1.0 and 1.4. The moderate perfusion pathology produces values between 0.95 and 1.0. Severe perfusion pathology corresponds to the values between 0.6 and 0.95. Extremely low TPR values below 0.6 are hardly observed. We consider the value 0.2 as complete blocking of the perfusion.

In order to use TPR as data for outflow boundary conditions, one should define a mapping between terminal points of CA network and perfusion zones. At least one terminal artery should be assigned to every microvascular territory. Unfortunately, the quality of the CT scans makes it impossible to segment all needed arteries in many cases. In the available case (see Section 1.3) we have managed to extract only ten terminal arteries (see Fig. 2). Thus, at least six arteries were missing. We assume that the missing arteries are not visible on CT images due to the low resolution. We generated them synthetically. We created synthetic arteries which originate from the closest points in the coronary network and ends up in the centre of the appropriate perfusion zone (see dotted lines in Fig. 2). The diameter of the synthetic arteries is prescribed to be equal to the diameter of the smallest of the segmented arteries

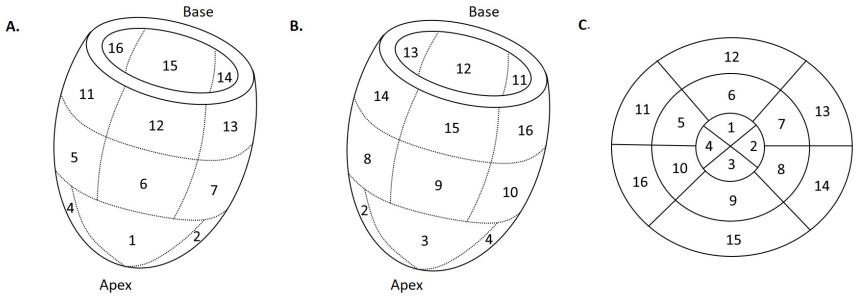

Figure 1. Zonal decomposition of the left ventricle: A is front view, B is rear view, C depicts all zones as a diagram (LV apex is in the center, LV base is on the sides).

(excluding stenosed parts). As a result, each perfusion territory of LV has a corresponding terminal artery.

Finally, we associate each terminal end of LCA branches with the closest territory of LV. If any two arteries end up in the same zone, we choose the artery nearest to the centre of the zone. Another artery is prescribed to the nearest neighbour territory.

The outflow boundary conditions assume that a terminal artery with index k is connected to the venous pressure reservoir with the pressure $p_{\text{veins}} = 8$ mmHg by the hydraulic resistance R_k. It is described by Poiseuille pressure drop condition

$$p_k(t, L_k) - p_{\text{veins}} = R_k A_k(t, L_k)\, u_k(t, L_k). \tag{1.8}$$

Compression of the terminal coronary arteries during systole by myocardium is an important feature of the coronary haemodynamics. To account for the compression, we set $R_k = R_k(t)$ for the boundary condition (1.8) in the terminal coronary arteries. Similar to our previous works [10, 9, 2] we assume, that the dimensionless time profile of $R_k(t)$ is the same as the dimensionless time profile of the cardiac output (1.6).

$$R_k(t) = \begin{cases} R_k + (R_k^{\max} - R_k)\sin\left(\dfrac{\pi t}{\tau}\right), & 0 \leqslant t \leqslant \tau \\ R_k, & \tau < t \leqslant T. \end{cases} \tag{1.9}$$

The peak value of the peripheral resistance during systole is set to $R_k^{\max} = 3R_k$, where R_k is the terminal resistance during diastole. It leads to complete blocking of the outflow. The base hyperemic diastolic value of the peripheral resistance is set to $R_k^{\text{hyp}} = 0.3R_k$. This value corresponds to clinical observations and our previous practice [8, 2].

The values of R_k are set by the following algorithm. We assume, that the total arterio-venous resistance R_{total} of the systemic circulation produces the pressure drop $\Delta P = P_{\text{mean}} - p_{\text{veins}}$, where P_{mean} is the mean blood pressure of the patient. Thus

$$R_{\text{total}} = \frac{\Delta P}{Q_{CO}} \tag{1.10}$$

where Q_{CO} is average cardiac output

$$Q_{CO} = \mathrm{SV} \cdot T^{-1}. \tag{1.11}$$

Then we divide R_{total} between the terminal resistance of the aorta $R_a = R_{\text{total}}/0.05$ and the total terminal resistance of the CAs $R_{\text{cor}} = R_{\text{total}}/0.95$. These values produce the ratio of CBF to CO about 3–6%. The total hydraulic resistance of coronary network R_{cor} is divided depending on the diameters of coronary arteries according to Murray's law with the power 2.27 [2]. The resulting base values of terminal resistances R_k are prescribed to each terminal branch, including synthetic vessels.

Finally, we update the base values of the terminal resistances R_k with respect to the measured TPR values. Qualitatively lower TPR values correspond to impaired perfusion and greater hydraulic resistance of the perfusion territory. Thus we multiply each base resistance R_k by a coefficient α_k:

$$\alpha_k = \begin{cases} 1, & \mathrm{TPR} \geqslant 1.4 \\ a + b\exp\left(c \cdot TPR_k\right), & \mathrm{TPR} < 1.4 \end{cases} \tag{1.12}$$

where TPR_k is a TPR value of corresponding LV zone. We set the values of a, b, and c so that $\alpha_k = 1$ for $TPR_k = 1.4$ and $\alpha_k = 4$ for $TPR_k = 0.2$

$$a = 2 + \frac{2}{\sqrt{3}}, \qquad b = \sqrt{\frac{(4-a)^3}{2-a}}, \qquad c = 5\ln\frac{4-a}{b}. \tag{1.13}$$

This makes blood flow through a segment with TPR < 0.2 negligibly small. In addition we set $\alpha_k = 2$ for $TPR_k = 0.6$ to designate clinically accepted borderline value of TPR. Exponential function grows slowly from $TPR_k = 1.4$ to $TPR_k = 1.0$ and grows faster from $TPR_k = 1.0$ to $TPR_k = 0.6$, which corresponds to clinical practice.

Correction of outflow boundary condition (1.12) increases peripheral resistance in the regions with low TPR, which simulates microcirculation pathology. We keep RCA branches in the model to increase the accuracy of the LCA portion of hydraulic resistance and blood flow.

1.3. Patient data

This study involves anonymous data from a single 73 years old patient with ischemic heart disease. The patient underwent contrast-enhanced coronary CT as well as rest and adenosine-enabled stress CT perfusion (CTP). The CT data of the large coronary arteries were processed by a previously developed segmentation algorithm [24, 26, 7]. The coronary perfusion was estimated by CTP images. CT scanner (Canon Aquilion ONE) calculated TPR for sixteen zones of the LV wall both for the rest and stress conditions. Figure 2 shows the extracted structure of the coronary network. Table 1 contains geometric parameters and CTP data.

Table 1. Parameters of the LCA and its branches: l is length, d is diameter, Zone is the index of corresponding TPR segment (see Fig. 1), TPR_{rest} is TPR value at natural physiological conditions, TPR_{stress} is TPR at hyperemic conditions which were produced by the adenosine administration.

No.	l (mm)	d (mm)	Zone	TPR_{rest}	TPR_{stress}
1	10.5	3.3	—	—	—
2	25.0	3.7	—	—	—
3	7.8	1.3	—	—	—
4	8.6	3.4	—	—	—
5	4.9	1.9	—	—	—
6	24.4	3.3	—	—	—
7	2.4	2.6	—	—	—
8	12.4	2.7	—	—	—
9	6.5	0.4	—	—	—
10	62	1.9	—	—	—
11	9.7	1.3	4	1.22	1.28
12	9.9	0.7	1	1.03	1.05
13	15.3	1.3	6	0.95	0.93
14	6.7	2.5	5	1.06	1.08
15	36.1	3.5	—	—	—
16	57.4	2.3	—	—	—
17	11.1	2.1	—	—	—
18	2.3	1.7	—	—	—
19	27.8	2.5	—	—	—
20	34.3	2.3	3	1.49	1.34
21	21.1	2.5	2	1.19	1.20
22	39.5	2.5	—	—	—
23	5.4	2.2	8	1.18	1.41
24	15.2	1.2	9	1.12	1.13
25	57.4	2.3	—	—	—
26	14.6	1.1	13	1.21	1.39
27	20.1	1.6	7	1.02	1.10
28	20.3	0.7	12	1.21	1.33
29	15.6	0.7	11	1.23	1.25
30	46.8	0.7	16	1.25	1.27
31	17.5	0.7	10	1.15	1.13
32	38.3	0.7	15	1.00	1.12
33	17.4	0.7	14	1.13	1.22

Table 2. Parameters of RCA and its branches: l is length, d is diameter.

No.	l, mm	d, mm
1	52.3	3.8
2	68.6	3.2
3	43.2	2.1
4	43.4	2.1
5	58.1	2.3

The patient was diagnosed with a series of epicardial stenoses in the left anterior descending artery (LAD). The proximal third of LAD contained two calcium atherosclerosis plaques which produce stenoses of 50% and 60% degree in the vascular segments 3 and 5 (see Fig. 1). In what follows, we refer to stenosis degree as a local

decrease of the diameter relative to the neighbour healthy part of the vessel. Another 85% degree stenosis was located in a distal part of the LAD in the vascular segment 9 (see Fig. 2). FFR of the vascular segment 9 was invasively measured before stent placement. It was equal to 0.43. CFR data were unavailable.

Aortic root was simulated as a vessel with the length set to 5 cm and diameter set to 2.3 cm. Aorta was simulated as a single vessel with the length set to 80 cm and diameter set to 2.17 cm. Parameters of LCA and RCA are presented in Tables 1 and 2.

2. Results

First we study the importance of the microvascular impairment to the accuracy of the FFR simulations. Let us compare the results of two simulations. In the first computational experiment, all TPR values are set to 1.4, i.e., the terminal hydraulic resistance is set to the initial base values at all terminal points regardless of CTP data. In the second series TPR values from Table 1 at stress conditions are used to calculate multipliers according to (1.12). We set stress TPR values by virtue of the fact that invasive FFR measurements are also performed after adenosine administration which is exactly the same as for the stress TPR measurements. The simulated values of FFR in the first and second cases are 0.39 and 0.41, respectively. The measured value of FFR was 0.43. Thus the relative error of simulated FFR is 9.3% and 4.7%, respectively. We have a substantially lower error when using patient TPR data.

In the second group of simulations, we study the sensitivity of FFR, CFR, and iFR to TPR in the distal territories (zones 1 and 4 in Figs. 1 and 2). In the first series, we change both stress and rest TPR values in zones 1 and 4 from 0.2 to 1.4 simultaneously and calculate FFR and CFR in each case. In these simulations, we use stress TPR values from Table 1 for the remaining zones to calculate FFR and hyperemic blood flow through stenosis for CFR. We use rest TPR values for the remaining zones to calculate blood flow in quiet conditions (at rest) for CFR and pressure over wave-free periods for iFR. In the second series of numerical experiments, we simulate stenting by removing stenosis in vessel 9 and recalculate FFR, CFR, and iFR for the same TPR values as in the first series.

The results are presented in Fig. 3. One can see that in the presence of the 85% stenosis in vascular segment 9 all indices increase significantly along with the decrease of TPR. It means that the lack of data on microcirculation pathology may be a reason of the substantial underestimation of the haemodynamic significance of a stenosis by noninvasive computational tools. This result supports clinical findings concluding that FFR can be artificially elevated in patients with microvascular dysfunction, leading to an underestimation of lesion severity [16].

From Fig. 3 one can also observe that in healthy conditions without stenosis, all indices demonstrate minor variations in the wide range of all possible TPR values. It means that revascularization improves haemodynamic indices even in the cases of impaired perfusion. FFR, CFR, and iFR evaluate the blood flow conditions in

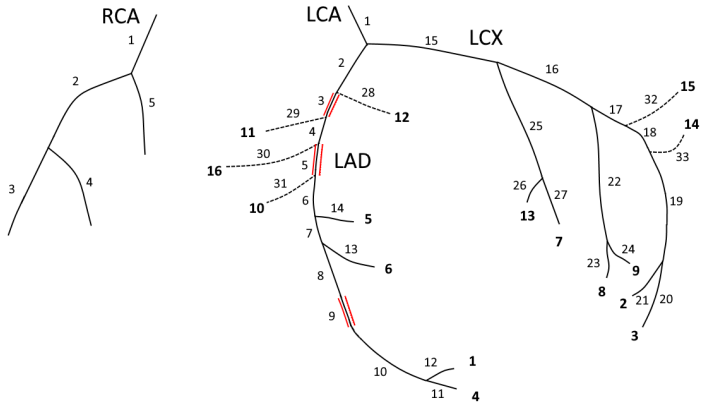

Figure 2. The structure of RCA and LCA. Bold numbers correspond to the LV perfusion zones (see Fig. 1). Dotted lines designate synthetic vessels. Vessels 3, 5, and 9 of LCA have stenoses.

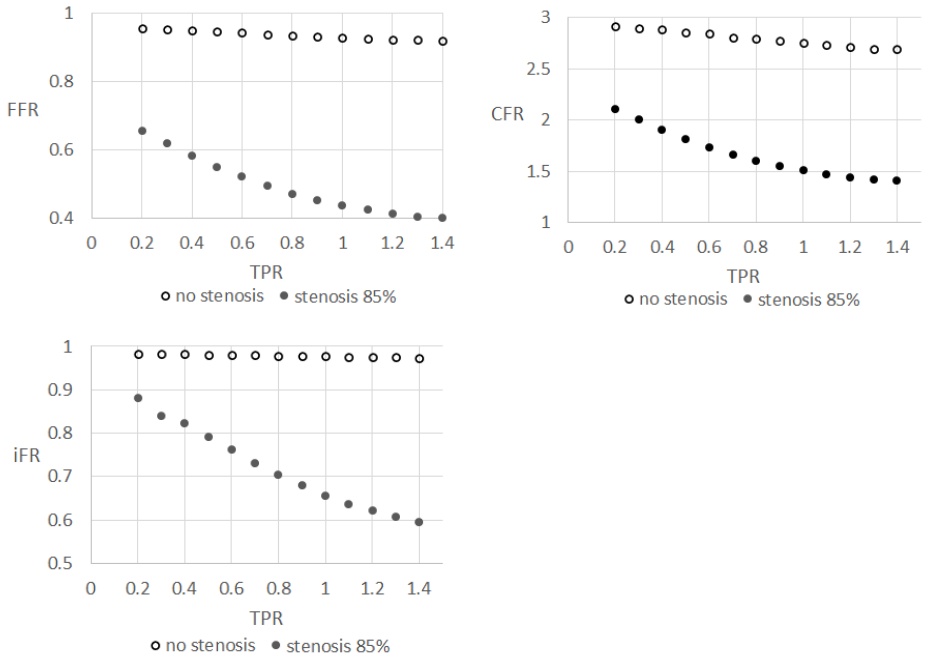

Figure 3. Calculated FFR, CFR, and iFR with and without stenosis for various TPR in zones 1 and 4 (see Fig. 2).

large coronary vessels regardless of microcirculation state. These indices may be high even if the coronary blood flow is dangerously low.

We should note that the stress and rest TPR values of our patient (see Table 1) are similar. The only problematic sector is zone 6 in both cases. This is the reason we changed TPR values for both stress (hyperemic) and rest conditions in our previous

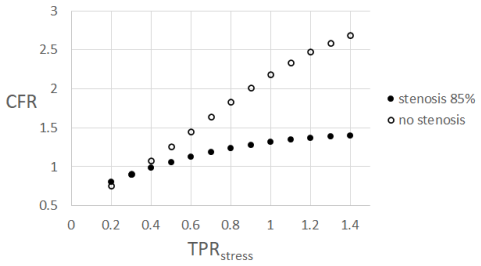

Figure 4. Calculated CFR with and without stenosis for various stress TPR in zones 1 and 4 (see Fig. 2). Rest TPR were fixed and taken from patient data (see Table 1).

calculations (Fig. 3). We assumed that microcirculation dysfunction manifests itself similarly under stress and at rest. However, in most cases perfusion impairment hinders hyperemic response of coronary haemodynamics while leaving rest state almost unaffected [12]. This can have a drastic effect on CFR, since CFR is the ratio between hyperemic and nonhyperemic (rest) blood flows. Figure 4 shows CFR values for various stress TPR values. Rest TPR values are the same for all calculations. As one can see, CFR behaviour changes compared to Fig. 3: CFR decreases with increased microcirculation dysfunction.

Finally, we study FFR, CFR, and iFR sensitivity to the variations of TPR in the neighbour territories. We change TPR values in zones 5 and 6 from 0.2 to 1.4 and calculate FFR, CFR, and iFR with and without stenosis in vascular segment 9 in each case similar to the previous simulations. We observe, that the maximum relative difference in all indices for all cases is less than 3%. Thus, we conclude that haemodynamic indices are not sensitive to the TPR values in the neighbour territories.

3. Conclusion

We have demonstrated that the effectiveness of coronary revascularization should be evaluated based on CT and CTP data. Healthy values of FFR after the stenotic treatment may be observed after ineffective revascularization, which may lead to a false negative decision. Myocardial perfusion impairment plays a significant role in the correct estimation and interpretation of haemodynamic indices across the stenotic regions of CAs before stenotic treatment by noninvasive computational techniques. This method is almost not sensitive to the post treatment analysis.

This is just a pilot study since we consider a single case. More clinical cases are required for the validation and development of a robust computational tool for practical usage.

In the present work, we utilize CT perfusion images and TPR values to assess myocardial perfusion. The other methods, such as PET (Positron Emission Tomography) perfusion, SPECT (Single Photon Emission Computed Tomography) perfusion, give more accurate 3D distribution of myocardial blood flow and can increase effectiveness.

The advantage of the presented approach is the availability of TPR perfusion assessment in everyday practice. Since we are also performing coronary CT to extract the structure of large coronary arteries, CT perfusion does not require additional equipment. It simplifies procedures for both patients and clinicians.

Acknowledgements

The authors acknowledge the staff of Sechenov University especially Nina Gagarina and Ekaterina Fominykh for patient-specific FFR and CTP data and Alexander Danilov for the fruitful discussion.

References

1. P. G. Camici and M. Magnoni, How important is microcirculation in clinical practice? *Eur. Heart J. Suppl.* **21** (2019), B25–B27.
2. J. M. Carson, S. Pant , C. Roobottom, R. Alcock, P. J. Blanco, C. A. Carlos Bulant, Y. Vassilevski, S. Simakov, T. Gamilov, R. Pryamonosov, F. Liang, X. Ge, Y. Liu, and P. Nithiarasu, On-invasive coronary CT angiography-derived fractional flow reserve: A benchmark study comparing the diagnostic performance of four different computational methodologies. *Int. J. Numer. Methods Biomed. Engrg.* **35** (2019), No. 10, e3235.
3. J. M. Carson, C. Roobottom, R. Alcock, and P. Nithiarasu, Computational instantaneous wave-free ratio (IFR) for patient-specific coronary artery stenoses using 1D network models. *Int. J. Numer. Methods Biomed. Engrg.* **35** (2019), No. 11, e3255.
4. A. Coenen, M. M. Lubbers, A. Kurata, A. Kono, A. Dedic, R. G. Chelu, M. L. Dijkshoorn, A. Rossi, R. M. van Geuns, and K. Nieman, Diagnostic value of transmural perfusion ratio derived from dynamic CT-based myocardial perfusion imaging for the detection of haemodynamically relevant coronary artery stenosis. *Eur. Radiol.* **27** (2017), No. 6, 2309–2316.
5. A. Coenen, A. Rossi, M. M. Lubbers, A. Kurata, A. K. Kono, R. G. Chelu, S. Segreto, M. L. Dijkshoorn, A. Wragg, R.-J. M. van Geuns, F. Pugliese, and K. Nieman, Integrating CT myocardial perfusion and CT-FFR in the work-up of coronary artery disease. *JACC: Cardiovasc. Imaging* **10** (2017), No. 7, 760–770.
6. R. C. Cury, T. A. Magalhes, A. T. Paladino, A. A. Shiozaki, M. Perini, T. Senra, P. A. Lemos, R. C. Cury, and C. E. Rochitte, Dipyridamole stress and rest transmural myocardial perfusion ratio evaluation by 64 detector-row computed tomography. *J. Cardiovasc. Comp. Tomography* **5** (2011), No. 6, 443–448.
7. A. Danilov, Yu. Ivanov, R. Pryamonosov, and Yu. Vassilevski, Methods of graph network reconstruction in personalized medicine. *Int. J. Numer. Methods Biomed. Engrg.* **32** (2016), No. 8, e02754.
8. T. M. Gamilov, P. Yu. Kopylov, R. A. Pryamonosov, and S. S. Simakov, Virtual fractional flow reserve assessment in patient-specific coronary networks by 1D haemodynamic model. *Russ. J. Numer. Anal. Math. Modelling* **30** (2015), No. 5, 269–276.
9. T. Gamilov, P. Kopylov, M. Serova, R. Syunyaev, A. Pikunov, S. Belova, F. Liang, J. Alastruey, and S. Simakov. Computational analysis of coronary blood flow: The role of asynchronous pacing and arrhythmias. *Mathematics* **8** (2020), No. 8, 1205.
10. T. M. Gamilov, F. Y. Liang, and S. S. Simakov, Mathematical modeling of the coronary circulation during cardiac pacing and tachycardia. *Lobachevskii J. Math.* **40** (2019), No. 4, 448–458.
11. T. Gamilov and S. Simakov, Blood flow under mechanical stimulations. *Advances in Intelligent*

Systems and Computing, Vol. 1028 (2020), 143–150.

12. X. Ge, Y. Liu, S. Tu, S. Simakov, Y. Vassilevski, and F. Liang, Model-based analysis of the sensitivities and diagnostic implications of FFR and CFR under various pathological conditions. *Int. J. Numer. Methods Biomed. Engrg.* (2019), e3257.
13. R. T. George, A. Arbab-Zadeh, J. M. Miller, K. Kitagawa, H. J. Chang, D. A. Bluemke, L. Becker, O. Yousuf, J. Texter, A. C. Lardo, and J. A. Lima, Adenosine stress 64- and 256-row detector computed tomography angiography and perfusion imaging: a pilot study evaluating the transmural extent of perfusion abnormalities to predict atherosclerosis causing myocardial ischemia. *Circulation. Cardiovasc. Imaging* **2** (2009), No. 3, 174–182.
14. K. L. Gould, R. L. Kirkeeide, and M. Buchi, Coronary flow reserve as a physiologic measure of stenosis severity. *J. Amer. Coll. Cardiol.* **15** (1990), No. 2, 459–474.
15. A. R. Ihdayhid, T. Sakaguchi, J. J. Linde, M. H. Srgaard, K. F. Kofoed, Y. Fujisawa, J. Hislop-Jambrich, N. Nerlekar, J. D. Cameron, R. K. Munnur, M. Crosset, D. Wong, S. K. Seneviratne, and B. S. Ko, Performance of computed tomography-derived fractional flow reserve using reduced-order modelling and static computed tomography stress myocardial perfusion imaging for detection of haemodynamically significant coronary stenosis. *Europ. Heart J. Cardiovasc. Imaging* **19** (2018), No. 11, 1234–1243.
16. A. Jeremias, A. J. Kirtane, and G. W. Stone, A test in context: Fractional Flow Reserve: accuracy, prognostic implications, and limitations. *J. Amer. Coll. Cardiol.* **69** (2017), No. 22, 2748–2758.
17. E. W. Lo, L. J. Menezes, and R. Torii, On outflow boundary conditions for CT-based computation of FFR: Examination using PET images. *Medical Engineering & Physics* **76** (2020), 79–87.
18. N. H. J. Pijls, B. Bruyne, K. Peels, P. H. van der Voort, H. J. R. M. Bonnier, J. Bartunek, and J. J. Koolen, Measurement of Fractional Flow Reserve to Assess the Functional Severity of Coronary-Artery Stenoses. *New England J. Medicine* **334** (1996), No. 26, 1703–1708.
19. A. Ruiz-Muoz, F. Valente, L. Dux-Santoy, A. Guala, G. Teixid-Tur, L. Galin-Gay, L. Gutirrez, R. Fernndez-Galera, G. Casas, T. Gonzlez-Alujas, I. Ferreira-Gonzlez, A. Evangelista, and J. Rodrguez-Palomares, Diagnostic value of quantitative parameters for myocardial perfusion assessment in patients with suspected coronary artery disease by single- and dual-energy computed tomography myocardial perfusion imaging. *IJC Heart & Vasculature* **32** (2021), 100721.
20. G. Sambuceti, A. L'Abbate, and M. Marzilli, Why should we study the coronary microcirculation? *Amer. J. Physiol.-Heart Circul. Physiol.* **279** (2000), No. 6, H2581–H2584.
21. S. Seitun, C. De Lorenzi, F. Cademartiri, A. Buscaglia, N. Travaglio, M. Balbi, and G. P. Bezante, CT myocardial perfusion imaging: A new frontier in cardiac imaging. *BioMed Research International* (2018), 7295460.
22. S. Sen, J. Escaned, I. S. Malik, G. W. Mikhail, R. A. Foale, R. Mila, J. Tarkin, R. Petraco, C. Broyd, R. Jabbou, A. Sethi, C. S. Baker, M. Bellamy, M. Al-Bustami, D. Hackett, M. Khan, D. Lefroy, K. H. Parker, A. D. Hughes, D. P. Francis, C. Di Mario, J. Mayet, and J. E. Davies, Development and validation of a new adenosine-independent index of stenosis severity from coronary wave-intensity analysis: results of the ADVISE (ADenosine Vasodilator Independent Stenosis Evaluation) study. *J. Amer. Coll. Cardiol.* **59** (2012), No. 15, 1392–1402.
23. S. Simakov, Spatially averaged haemodynamic models for different parts of cardiovascular system. *Russ. J. Numer. Anal. Math. Modelling* **35** (2020), No. 5, 285–294.
24. Yu. V. Vassilevski, A. A. Danilov, T. M. Gamilov, S. S. Simakov, Y. A. Ivanov, and R. A. Pryamonosov, Patient-specific anatomical models in human physiology. *Russ. J. Numer. Anal. Math. Modelling* **30** (2015), No. 3, 185–201.
25. Y. V. Vassilevski V. Y. Salamatova, and S. S. Simakov, On the elasticity of blood vessels in one-dimensional problems of haemodynamics. *Comput. Math. Math. Phys.* **55** (2015), No. 9, 1567–1578.

26. Yu. Vassilevski, M. Olshanskii, S. Simakov, A. Kolobov, and A. Danilov, *Personalized Computational Haemodynamics: Models, Methods, and Applications for Vascular Surgery and Antitumor Therapy*. Academic Press, 2020.

27. M. M. Zaman, S. S. Haque, M. A. Siddique, S. Banerjee, C. M. Ahmed, A. K. Sharma, M. F. Rahman, M. H. Haque, A. I. Joarder, A. U. Sultan, and K. Fatema, Correlation between severity of coronary artery stenosis and perfusion defect assessed by SPECT myocardial perfusion imaging. *Mymensingh Medical J.* **19** (2010), No. 4, 608–613.